Article

In situ Electrochemical Generation of Electrochemiluminescent Silver Naonoclusters on Target-cycling Synchronized Rolling Circle Amplification Platform for MicroRNA Detection

Anyi Chen, Shaoyong Ma, Ying Zhuo, Yaqin Chai, and Ruo Yuan

Anal. Chem., **Just Accepted Manuscript** • DOI: 10.1021/acs.analchem.5b04578 • Publication Date (Web): 17 Feb 2016

In situ Electrochemical Generation of Electrochemiluminescent Silver Naonoclusters on Target-cycling Synchronized Rolling Circle Amplification Platform for MicroRNA Detection

Anyi Chen, Shaoyong Ma, Ying Zhuo*, Yaqin Chai, Ruo Yuan*

Key Laboratory of Luminescent and Real-Time Analytical Chemistry (Southwest University), Ministry of Education, College of Chemistry and Chemical Engineering, Southwest University, Chongqing 400715, China

* Corresponding authors at: Tel.: +86 23 68252277, fax: +86 23 68253172.
E-mail addresses: yingzhuo@swu.edu.cn (Y. Zhuo), yuanruo@swu.edu.cn (R. Yuan).

ABSTRACT

Based on a novel target-cycling synchronized rolling circle amplification (RCA) as signal amplification strategy and *in situ* electrochemical generation of silver nanoclusters (Ag NCs) as signal probes, an ultrasensitive and simple electrochemiluminescence (ECL) biosensor was proposed for microRNA (miRNA) detection. It was worth mentioning that the circular template was subtly designed to consist of a guanine-rich (G-rich) region and a binding region for realizing target-cycling synchronized RCA. In the presence of target miR-21, the binding region hybridized with the primer and the target miR-21 to form a ternary "P" junction structure, and then the RCA was triggered from the 3′-end of the primer. Along with the proceeding of RCA, the target miR-21 was released and participated into another trigger of the RCA. On account of the G-rich region in the circular template, the product DNA of the target-cycling synchronized RCA possessed tandem periodic cytosine-rich (C-rich) sequences, which acted as ligands to further *in situ* electrochemically generate silver nanoclusters (Ag NCs) as ECL signal probes. As expected, the obtained ECL intensity depended on the amount of the Ag NCs, which was positively related to the concentration of the target miR-21. The ECL assay for miR-21 detection demonstrated excellent linear respond to a concentration variation from 100 aM to 100 pM and limit of detection down to 22 aM.

INTRODUCTION

Electrochemiluminescence (ECL) has attracted explosive interest in analytical methodology due to its unique advantages of low background signal, simplified optical setup and high sensitivity.[1-3] Since the ECL nanomaterials of quantum dots was first reported in 2002, [4] it has become more and more fascinating because of their unique quantum size dependent optical and electrochemical properties.[5,6] However, most quantum dots used in ECL studies exhibited the inherent toxicity due to the existence of toxic metal ions (e.g., cadmium and lead), which limited their applications in bioassays. Thus, it is of great value to develop novel low-toxicity or nontoxic ECL nanomaterials. Noble metal nanoclusters, including gold nanoclusters (Au NCs) and silver nanoclusters (Ag NCs) attracted substantial research effort on the basis of their low toxicity, good biocompatibility, and excellent stability.[7-15] Previous works have reported the bovine serum albumin (BSA)-stabilized Au NCs and Ag NCs were successively synthesized by a facile one-pot method and applied in the cathodic ECL biosensing assay for the biomolecule detection.[16,17] Summarized from the above works, the synthesized noble metal nanoclusters were commonly applied in solution-phase ECL, which caused several disadvantages of the high background signal and complicated experimental design compared with noble metal nanoclusters-based solid-state ECL. In this perspective, developing an efficient and convenient method to label noble metal nanoclusters is still highly desired in the ECL biosensing construction.

Recently, DNA-stabilized Ag NCs, integrating the luminescent properties of Ag

NCs and the biochemical specificity of nucleic acid, have been widely applied as multifunctional biolabels.[18-21] Willner′s group developed a photoluminescent platform for genes detection based on the stable and diverse optical properties of DNA-stabilized Ag NCs.[22] Orbach and coworkers utilized the excellent self-assembly property of DNA-stabilized Ag NCs to prepare the photoluminescent Ag NCs-functionalized nanowires.[23] Inspired by the above superiority of the DNA ligands, DNA-stabilized Ag NCs provided a promising prospect for the development of biolabels. However, the DNA-stabilized Ag NCs were almost prepared in homogeneous aqueous solution with the help of reductants (e.g., $NaBH_4$) in advance, which suffered the problems of complicated operation procedure, inconvenient storage and increased risk of analysis errors.

Rolling circle amplification (RCA) is an isothermal amplification approach involving a circular template to produce tandem periodic oligonucleotides, which have been used for in vitro cloning, library construction, and other molecular biology applications.[24-29] Tang′s group developed a high specific and ultrasensitive fluorescent assay for microRNA (miRNA) detection by designing the target miRNA as the primer to trigger the rolling circle reaction.[30] Han and coworkers proposed a target-cycling strategy combined with RCA in order to achieve a cascade signal amplification.[25] However, it was easy to see that the target-cycling reaction and RCA were stepwise executed, resulting in the tedious operation and relatively low RCA efficiency.

Herein, we firstly proposed a novel signal amplification pattern of synchronous target-cycling reaction and RCA, in which the amplified products acted as ligands for

further electrochemical generation of Ag NCs. Based on the *in situ* electrochemical generated DNA-stabilized Ag NCs as a novel ECL probes, an ultrasensitive and simple biosensor was constructed for miRNA detection. As exhibited in Scheme 1, the 5′-NH_2 modified primer was firstly fabricated on the gold electrode (GE) *via* molecular self-assembly. In the presence of target miRNA (miR-21), the circular template consisted of a G-rich region and a binding region hybridized with the target miR-21 and the primer to make up a ternary "P" junction structure. Then, RCA was triggered from the 3′-end of the primer to synthesize a double-stranded DNA based on the circular template. With the proceeding of RCA, the target miR-21 was released by the strand-displacement polymerization and triggered next RCA reaction. As a result, the target miR-21 circularly induced the RCA which realized synchronous target-cycling and RCA. Moreover, periodic C-rich ssDNA was created by the RCA due to the G-rich region of the circular template. After incubating with Ag NO_3 solution to form the stable cytosine-Ag^+-cytosine, the Ag NCs were *in situ* generated on the RCA-produced C-rich ssDNA *via* electrochemical reduction. In view of Ag NCs/$S_2O_8^{2-}$-based ECL system, the obtained ECL intensity increased with the increasing concentration of the target miR-21. Due to the high sensitivity of target-cycling synchronized RCA and the fast preparation of *in situ* electrochemically generated Ag NCs, the ECL biosensor achieved rapid and ultrasensitive detection of miR-21.

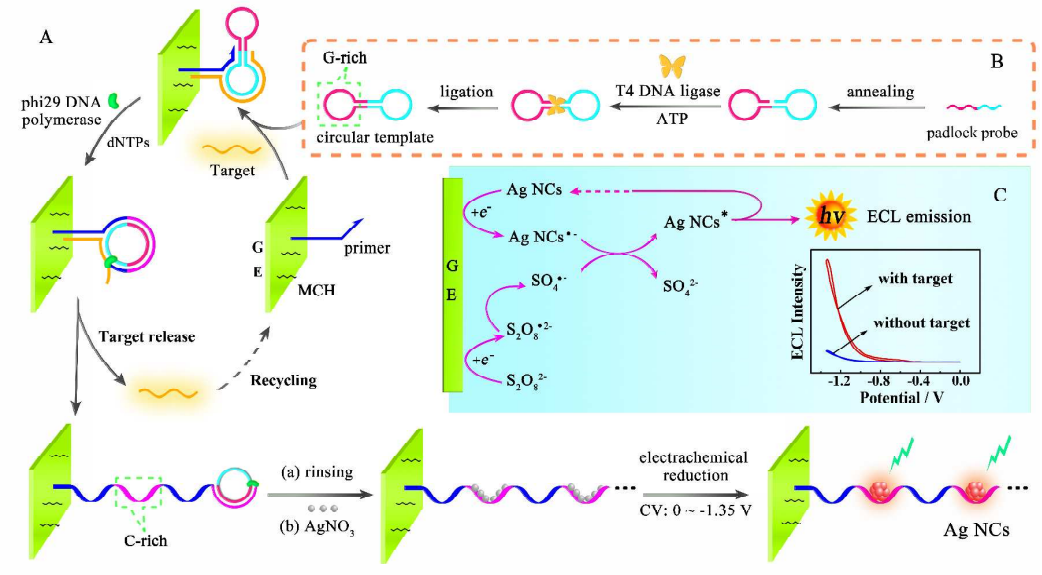

Scheme 1 Schematic illustration of (A) the principle of target-cycling synchronized RCA and *in situ* electrochemical generation of Ag NCs, (B) the preparation of the circular template, (C) the ECL mechanism of Ag NCs/$S_2O_8^{2-}$-based ECL system.

EXPERIMENTAL METHODS

Materials and reagents. HPLC-purified miRNA, T4 DNA ligase and 10×T4 DNA ligase reaction buffer were obtained from Takara Biotechnology Company Ltd. (Dalian, China). Phi29 DNA polymerase and 10×phi29 DNA polymerase reaction buffer were purchased from Thermo Fisher Scientific, Inc. (Waltham, Massachusetts, USA). The DNA oligonucleotides, diethy pyrocarbonate (DEPC) and the solution of deoxyribonucleoside triphosphate (dNTPs) mixture were purchased from Sangon, Inc. (Shanghai, China). The tumor cells were cultured by Well-Biology Co. (Changsha, China). Silver nitrate and other reagents used in this work were analytical reagent (A.R.) grade. The deionized water was purified by a water purification system with an electrical resistance of 18.2 MΩ·cm and then treated with autoclaving. DEPC solution (0.1 % v/v) was employed to create an RNase-free environment. The tips and tubes were RNase-free and did not require pretreatment to inactivate RNases.

The buffers involved in this work were prepared as follows: 10×T4 DNA ligase reaction buffer contained 660 mM Tris-HCl, 66 mM $MgCl_2$, 100 mM dithiothreitol (DTT) and 1 mM adenosine triphosphate (ATP). 10×phi29 DNA polymerase reaction buffer contained 330 mM Tris-acetate, 100 mM Mg-acetate, 660 mM K-acetate, 1% Tween 20 and 10 mM DTT. 0.1 M Phosphate Buffered Saline (PBS, pH 7.4) containing 5 mM $K_2S_2O_8$ was used as electrolyte for ECL measurement. 1×TE buffer (10 mM Tris-HCl, 1.0 mM ethylenediaminetetraacetic acid (EDTA), pH 8.0) was used for DNA oligonucleotides dissolution. Annealing buffer (10 mM Tris·HCl, 100 mM NaCl, 1 mM EDTA, pH 8.0) was used to obtain specific secondary structure for

circular template preparation.

The nucleotide sequences of the oligonucleotides used in this work were shown in Table 1.

Table 1. Sequence Information for the Nucleic Acids Used in This Study

name	sequences*(5′→3′)
miR-21	UAG CUU AUC AGA CUG AUG UUG A
miR-141	UAA CAC UGU CUG GUA AAG AUG G
miR-155	UUA AUG CUA AUC GUG AUA GGG GU
miR-199a	ACA GUA GUC UGC ACA UUG GUU A
primer	NH_2C_6-TCA ACA TAT CTG AC
padlock probe	p-AGC TTT AGT CAG CAG TCT GAT AAG CTA AAG CTT ATA ACA GGA GGA AGG AGG TGT TAT A

Apparatus. The ECL measurements were performed on a model MPI-A electrochemiluminescence analyzer (Xi'An Remax Electronic Science & Technology Co. Ltd., Xi′An, China) with a conventional three-electrode system used with Ag/AgCl (saturated KCl) as the reference electrode, a platinum wire as auxiliary electrode and a modified gold electrode (GE, Φ = 4 mm) as the working electrode in the experiment. Electrochemical measurement was carried out with a CHI660C electrochemistry workstation (Shanghai Chenhua Instruments, China). The surface appearance of Ag NCs was characterized by high resolution transmission electron microscopy (HRTEM, FEI Tecnai G20, FEI, Hillsboro, Oregon, USA) at an

acceleration voltage of 200 kV. UV-Vis absorption spectra were carried out on UV-2450 UV-Vis spectrophotometer (Shimadzu, Tokyo, Japan). Fluorescence spectra of Ag NCs were carried out on RF-5301PC spectrophotometer (Shimadzu, Tokyo, Japan) with a 150W Xenon lamp (Ushio Inc, Japan) as the excitation source at room temperature. Native polyacrylamide gel electrophoresis was performed with BG-verMIDI standard vertical electrophoresis apparatus (Baygene, Beijing, China). The gel imaging was implemented with a Bio-Rad Gel Doc™ XR+ System (Bio-Rad, Hercules, California, USA)

Preparation of circular template. The circular template was prepared *via* an intramolecular ligation. First, 1 μM of the padlock probe solution was prepared with the annealing buffer. Then the solution was heated to 95 ℃ for 10 min and slowly cooled down to room temperature for 4 h to ensure the formation of dumbbell-like secondary structure. After the addition of 1×T4 DNA ligase reaction buffer and T4 DNA ligase (1 U/μL), the reaction system was incubated over night at 16 ℃ to finish the intramolecular ligation. Finally, the reaction was terminated by a thermal treatment at 65 ℃ for 10 min, and the resultant products were stored at 4 ℃ for further use.

Fabrication of biosensor. First, the gold electrode (GE, Φ = 4 mm) was cleaned by immersion in a freshly prepared piranha solution (a 3:1 v/v mixture of concentrated H_2SO_4 and 30 % H_2O_2) for 30 min. After rinsing thoroughly with deionized water, the electrode was polished with 0.3 and 0.05 μm aluminum slurry and sequentially sonicated with deionized water, ethanol and deionized water for 5 min each to remove

residual alumina powder. The well-polished electrode was then electrochemically cleaned to remove any remaining impurities. Immediately, 10 μL the primer solution (2.5 μM, TE buffer) was dropped on the pretreated electrode and incubated for 12 h at room temperature. Finally, the electrode surface was rinsed with deionized water and blocked with 1 mM MCH for 2 h.

Target-cycling synchronized RCA. Briefly, 10 μL 1×reaction phi29 DNA polymerase buffer containing 1 nM target miRNA (miR-21 in this work), 100 nM the prepared circular template, 2.5 mM dNTPs mixture and 100 U/mL phi29 DNA polymerase was dropped on the biosensor and incubated for 6 h at 30 °C. Then deionized water was used to rinsing the biosensor to remove the unbound reagents. In the determination of calibration curves, target miRNA with different concentrations were added into the reaction solution, and other operations were as fore-mentioned.

ECL measurement procedure. To measure the ECL signal, the biosensor was incubated with 10 μL $AgNO_3$ solution (1 mM, pH 5.0) for 60 min after the target-cycling synchronized RCA. After rinsed with deionized water to remove the unbound silver ions, the potential from 0 ~ -1.35 V with scan rate of 100 mV/s was applied to the biosensor for *in situ* electrochemical generation of Ag NCs and ECL measurement in 0.1 M PBS (pH 7.4) containing 5 mM $K_2S_2O_8$.

Applications for practical samples detection. Human lung adenocarcinoma cells (A549) and human cervical cancer cells (Hela) were selected to perform the practical tests. After processed with cell counting, a column type commercial miRNA extraction kit was used to extract miRNAs from the cell samples with different

amounts. As a result, miRNAs were extracted from the samples and dissolved in 30 μL RNase-free water. Then, the extraction solutions were used for miR-21 detection with the biosensor.

Native polyacrylamide gel electrophoresis (PAGE). The samples were loaded into the notches of the freshly prepared native polyacrylamid gel (16 %), and electrophoresis was performed at 120 V for 120 min in 1×TBE buffer. After dying with ethidium bromide (EB), the gel was transferred to the Bio-Rad Gel Doc™ XR+ System for gel imaging.

RESULTS AND DISCUSSION

Native PAGE characterization of the target-cycling synchronized RCA. Native PAGE assay was implemented to verify the successful execution of the target-cycling synchronized RCA in response to the target miR-21. As shown in Figure 1, miR-21, the primer and the circular template in lane 1, 2, and 3, respectively, exhibited a distinct single band. The dim band of the primer was attributed to its short oligonucleotide sequence. Lane 4, 5, and 6 showed the PAGE results for the hybridization of primer/circular template, miR-21/circular template, and primer/miR-21/circular template, respectively. Lane 4 exhibited two distinct bands of the primer and the circular template, suggesting that the primer couldn't hybridize with the circular template in the absence of miR-21. However, miR-21 could hybridize with the circular template, which was confirmed by the band with mobility lower than the circular template in lane 5. What's more, two distinct bands with mobility lower than the circular template were observed in lane 6, indicating the

formation of primer/miR-21/circular template complex. Lane 7 and 8 displayed the PAGE results for the target-cycling synchronized RCA in the absence and in the presence of miR-21, respectively. As expect, no obvious band of RCA products, which exhibited a bright band with extremely low mobility in lane 8, was observed in lane 7, indicating that the target-cycling synchronized RCA was not triggered in the absence of target miR-21. Comparing the results of lane 7 to lane 8, the distinction sufficiently verified the specific response to the target miR-21 of the proposed target-cycling synchronized RCA.

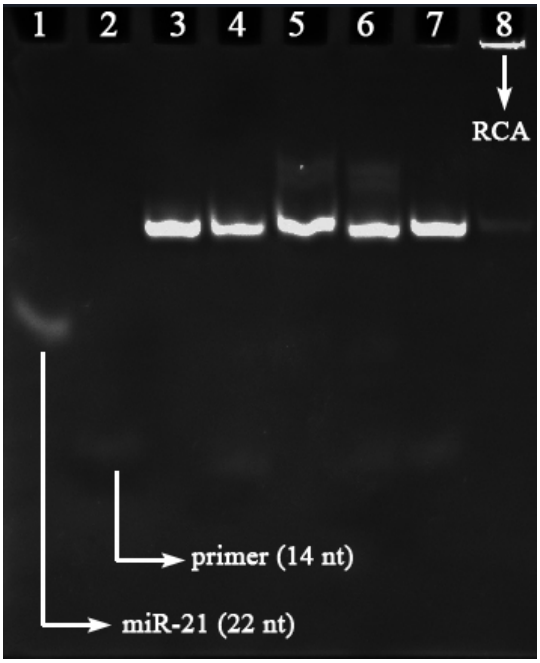

Figure 1 Native PAGE images of different samples. Lane 1: miR-21 (1 μM); Lane 2: the primer (1 μM); Lane 3: the circular template (1 μM); Lane 4: the mixture of the primer and the circular template; Lane 5: the mixture of miR-21(1 μM) and the circular template (1 μM), Lane 6: miR-21(1 μM), the primer (1 μM) and circular template (1 μM); Lane 7: RCA in the absence of miR-21 (1 μM the primer, 1 μM the

circular template, 2.5 mM dNTPs mixture, 100U/mL phi29 DNA polymerase and 1×phi29 DNA polymerase reaction buffer, incubated at 30°C for 12 h); Lane 8: RCA in the presence of miR-21 (1 μM miR-21, 1 μM the primer, 1 μM the circular template, 2.5 mM dNTPs mixture, 100U/mL phi29 DNA polymerase and 1×phi29 DNA polymerase reaction buffer, incubated at 30°C for 12 h).

HRTEM and optical spectrum characterization of the *in situ* generated Ag NCs on RCA-produced DNA. HRTEM was carried out to investigate the morphology and the size of the *in situ* generated Ag NCs on RCA-produced DNA. The typical HRTEM image (Figure 2A) demonstrated that the Ag NCs with an average diameter about 3 nm were uniformly distributed in the field of view. In order to further confirm the crystalline structure of the as-synthesized nanocluster, the enlarged HRTEM image was showed in the inset of Figure 2A. It could be seen that the metal core of about 1.5 nm in diameter was observed in the DNA-stabilized Ag NCs.

Figure 2B displayed the UV-Vis absorption spectra of the RCA-produced C-rich DNA (curve a) and the *in situ* generated DNA-stabilized Ag NCs (curve b). As shown in curve a, a distinct absorption peak was observed around 260 nm, which was the specific absorption peak of DNA. After the *in situ* generation of Ag NCs, the specific absorption peak became broader and had a slightly blue-shift of 10 nm comparing to that of DNA (curve b), suggesting the high affinity of the RCA-produced C-rich DNA to Ag NCs. Besides, due to the molecule-like characters of the electronic energy structure, metal nanoclusters were different from the larger metal nanoparticles with

surface plasmon resonance (SPR) characteristic absorption band. Here, the strong SPR around 400 nm of larger Ag nanoparticles couldn't be observed on the curve b, revealing the tiny size of the Ag NCs.

The luminescence of the Ag NCs was profiled with the photoluminescence (PL) spectra and the ECL spectra. Figure 2C depicted the PL spectra of the Ag NCs, which demonstrated the excitation peak at around 410 nm (curve a) and emission peak at 470 nm (curve b). The solution of the Ag NCs was almost colorless under ambient daylight but exhibited bright blue color when irradiated with a UV lamp (λ = 365 nm) (the insert in Figure 2C). Meanwhile, the ECL spectra were achieved with the help of the optical filters which were alternately set up between the photomultiplier and the electrochemical cell. As shown in Figure 2D, the ECL emission peak was located around 525 nm (curve a), which significantly differed from the emission peak of a typical $S_2O_8^{2-}/O_2$ ECL system (around 600 nm, curve b). The result manifested that the ECL signal came from the emission of Ag NCs rather than $S_2O_8^{2-}/O_2$ ECL system. The slight red shift from the PL spectrum to ECL spectrum of Ag NCs was attributed to the higher concentration used during the ECL experiments, internal filter effects (self-absorption), and instrument effects.[31-33]

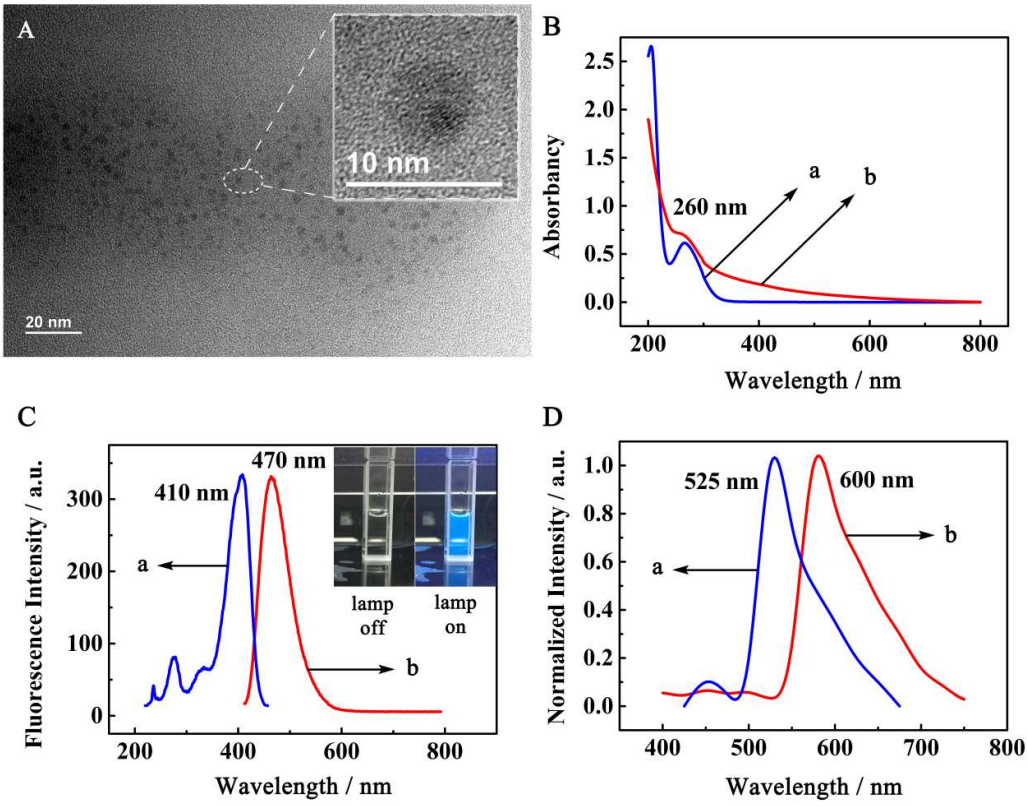

Figure 2 (A) HRTEM images of the Ag NCs *in situ* generated on RCA-produced C-rich DNA. The inset showed a close-up displaying the crystalline structure of an individual nanocluster. (B) UV-Vis absorption profiles of the RCA-produced DNA ligands (curve a) and DNA-stabilized Ag NCs (curve b). (C) PL excitation spectrum (curve a) and emission spectrum (curve b) of the Ag NCs. (D) Normalized ECL spectra of Ag NCs (curve a) and typical $S_2O_8^{2-}/O_2$ system (curve b). The ECL signals were measured in 0.1 M PBS (pH 7.4) containing 5 mM $K_2S_2O_8$ by scanning the potential from 0 to -1.35 V at a scanning rate of 100 mV/s.

Mechanism investigation of the Ag NCs ECL system. To investigate the ECL mechanism of the Ag NCs, ECL and CV were measured without and with the coreactant of $S_2O_8^{2-}$, respectively. As shown in Figure 3A, a feeble ECL emission

(about 10 a.u.) of the Ag NCs was observed with electrolyte solution of typical PBS (curve a1). The close-up of the CV curve between 0 ~ -1.0 V displayed a distinct reduction peak around -0.57 V (curve a2), which was attributed to the electrochemical process of Ag NCs + e^- → Ag NCs$^{\bullet-}$.[16,34,35] When the $S_2O_8^{2-}$ was added into the electrochemical cell, the ECL emission was noticeably raised to 2800 a.u. (Figure 2B, curve b1). The close-up of the CV curve showed that the reduction peak current was raised about 5 folds (insert of Figure 3B, curve b2), indicating that the electrochemically generated Ag NCs$^{\bullet-}$ were easily oxidized by $S_2O_8^{2-}$ to generate more Ag NCs. Therefore, a possible mechanism of the Ag NCs-based ECL system was proposed as shown in Scheme 1D.

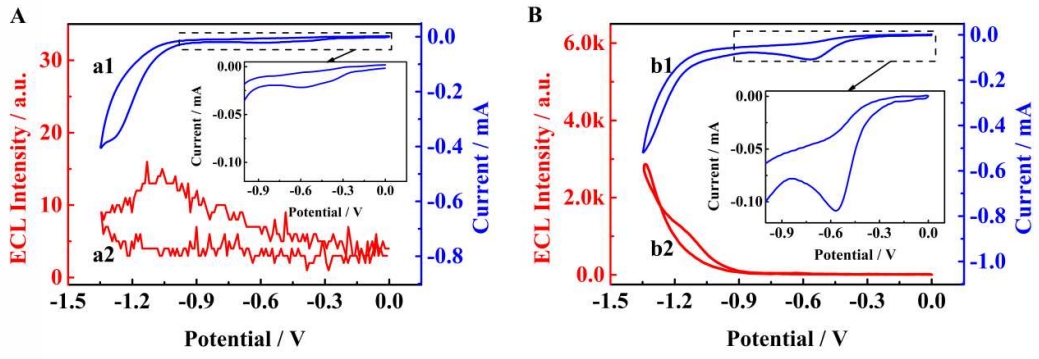

Figure 3 ECL responses (red line) and CVs (blue line) of the Ag NCs: (A) without $S_2O_8^{2-}$, (B) with $S_2O_8^{2-}$ (5 mM). The ECL signals were measured in 0.1 M PBS (pH 7.4) by scanning the potential from 0 to -1.35 V at a scanning rate of 100 mV/s.

Electrochemical characterization of the biosensor fabrication. To confirm the process of the ECL sensor fabrication, we employed the CV experiments to characterize different assembled electrodes in 5.0 mM $[Fe(CN)_6]^{3-/4-}$ solution. As shown in Figure 4A, a pair of the apparent redox peaks of $[Fe(CN)_6]^{3-/4-}$ can be

observed on the bare GE (curve a). After incubated with the primer solution on the bare GE surface, an obvious decrease in redox current was observed, suggesting that the immobilization of nucleic acid brought higher impedance of the electron transfer (curve b). Then MCH was used to block the nonspecific binding sites, the redox current further decreased (curve c). As expected, after target-cycling synchronized RCA being performed, the current responses declined, indicating ssDNA extended from 3′-end of the primer to create larger DNA molecule (curve d), which exaggerated the impedance of the biosensor. To further confirm the immobilization of the silver ions, CVs experiments were employed to characterize the biosensor after incubated with silver nitrate solution. As shown in Figure 3B, a pair of the apparent redox peaks of Ag^{+} was observed in the CV curves, indicating that the silver ions could be captured by the RCA-treated biosensor.[36]

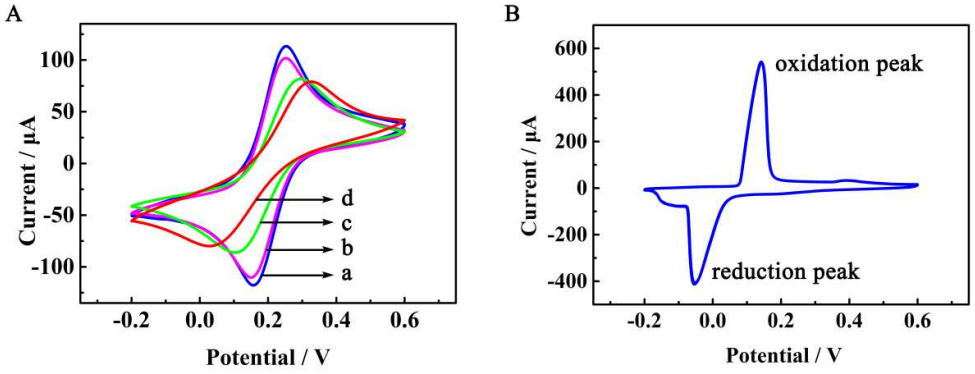

Figure 4 CVs at the (A): (a) bare GE, (b) primer/GE, (c) MCH/primer/GE, (d) RCA/MCH/primer/GE, and (B): *in situ* electrochemically generated AgNCs in 5.0 mM $[Fe(CN)_6]^{3-/4-}$ by scanning the potential from -0.2 to 0.6 V at a scan rate of 50 mV/s.

Detection of miR-21 with the biosensor. The performance of the proposed

biosensor was monitored by incubating with $AgNO_3$ solution (1 mM). The ECL intensity of the biosensor increases with increasing concentration of miR-21 (Figure 5A). The calibration plot shows a good linear relationship between ECL responses and the logarithmic value of miR-21 concentrations ranging from 100 aM to 100 pM with a correlation coefficient of 0.9984 (Figure 5B). The regression equation is I = 7905 + 413.0 lg(c/M) (where I stands for the ECL intensity and c stands for the concentration of miR-21) with a detection limit of 22 aM.[37] The comparison for existing miRNA detection methods demonstrates that this biosensor provides an easier and more effective way and a wider dynamic concentration response range to quantify miR-21 (Table 2).

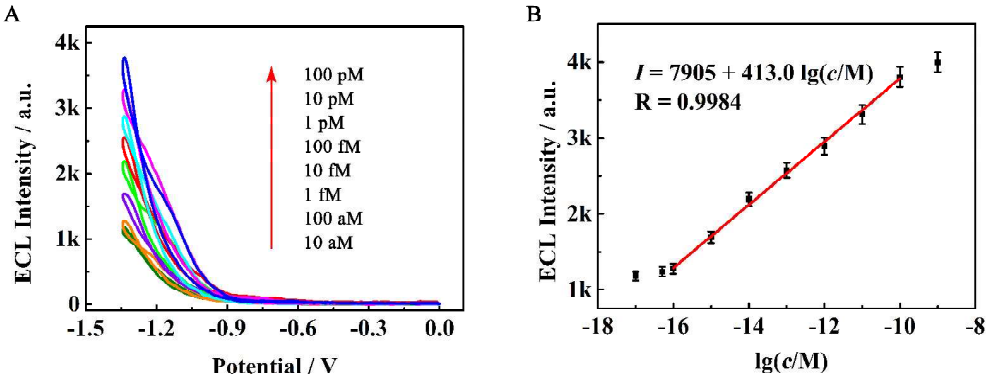

Figure 5 Sensitivity investigation of the proposed ECL biosensor with miR-21 as the model target. (A) ECL intensity-potential curves of the biosensor tested with different concentrations of miR-21. (B) The corresponding calibration curve of the biosensor for miR-21 assay. The ECL signals were measured in 0.1 M PBS (pH 7.4) containing 5 mM $K_2S_2O_8$ by scanning the potential from 0 to -1.35 V at a scanning rate of 100 mV/s.

Table 2 The comparison for Existing miRNA Detection Methods

methods	detection limit	dynamic rang	reference
Electrochemical	67 fM	100 fM – 10 nM	34
Electrochemical	8.2 fM	25 fM – 300 fM	38
Photoluminescent	0.5 pM	0.5 pM – 100 pM	26
Photoluminescent	0.6 fM	1 fM – 10 pM	39
ECL	not shown	1 fM – 10 pM	40
ECL	22 aM	100 aM –100 pM	this work

Selectivity of the miRNA biosensor. Three different miRNAs were used as interfering substances, including miR-141, miR-155 and miR-199a, to evaluate the selectivity and specificity of the present biosensor. As shown in Figure 6A, the contrast experiments were performed by using miR-141 (10 nM), miR-155 (10 nM) and miR-199a (10 nM), to replace miR-21 (100 pM) respectively. We could see that the ECL signal of miR-141, miR-155 and miR-199a did not exhibit any obvious increase compared with the blank. The mixture containing miR-21 (100 pM), miR-141 (10 nM), miR-155 (10 nM) and miR-199a (10 nM) was tested by the biosensor. Comparing the ECL response of the mixture with that of 100 pM miR-21 only, no remarkable difference was observed. They all indicated that the ECL intensity in the presence of miR-21 was much stronger than those of the others, which meant that miR-141, miR-155 and miR-199a had no obvious influence on the response to miR-21. The biosensor displayed good selectivity and specificity for the determination of miR-21.

Stability of the miRNA biosensor. Stability is of great importance to judge the

performance of the biosensor. In order to adequately investigate whether the biosensor could meet the needs of cyclic potential scan for long testing process, the stability of the proposed biosensor was studied under continuous scanning for 10 cycles in 0.1 M PBS (contain 5 mM $K_2S_2O_8$, pH 7.4). As shown in Figure 6B, the ECL peak intensity of the biosensor exhibited no obvious fluctuation (RSD = 1.961%) during the continuous scanning. The results suggested that the stability of the proposed biosensor was favorable.

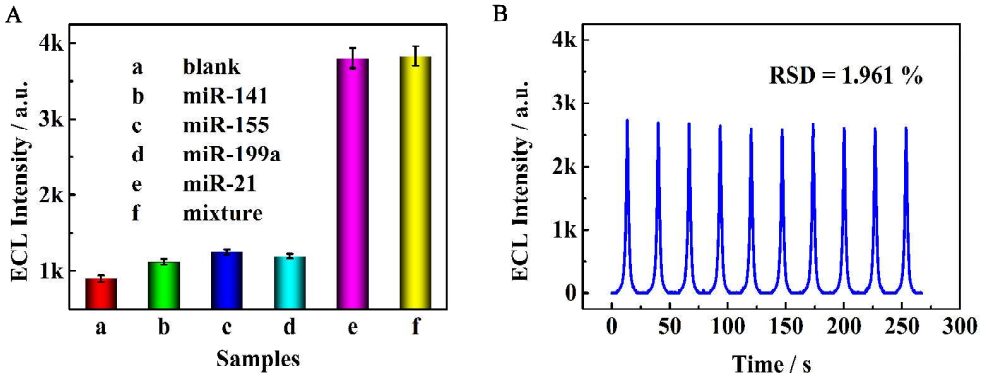

Figure 6 (A) Selectivity of the proposed ECL aptasensors with different targets: (a) blank, (b) 10 nM miR-141, (c) 10 nM miR-155, (d) 10 nM miR-199a, (e) 100 pM miR-21and (f) a mixture (containing 10 nM miR-141, 10 nM miR-155, 10 nM miR-199a and 100 pM miR-21). (B) Stability of the proposed ECL biosensor under a continuous cyclic potential scan for 10 cycles. The ECL signals were measured in 0.1 M PBS (pH 7.4) containing 5 mM $K_2S_2O_8$ by scanning the potential from 0 to -1.35 V at a scanning rate of 100 mV/s.

Application of the miRNA biosensor in tumor cells. To evaluate the capacity of the proposed biosensor applied in tumor cell extractions analysis, human lung adenocarcinoma cell line A549 (a cell line with high expression of miR-21) and

human cervical cancer cell line Hela (a cell line with low expression of miR-21) were selected to perform an ECL assay to measure the expression of miR-21. The cell samples were processed by a commercial miRNA extraction kit after cell counting. The sensitivities were explored by setting the cell concentrations as 10 cells to 10^6 cells. According to the results shown in Figure 7, the extraction of Hela cells caused slight increases in the ECL response when the cell concentrations increased from 10 cells to 10^4 cells, indicating the low expression of miR-21 in the Hela cells. While the extraction of A549 cells resulted in obvious ECL response to a concentration variation from 10 cells to 10^6 cells, suggesting the high expression of miR-21 in the A549 cells. The comparisons manifested the overexpression of miR-21 in the A549 cells rather than the Hela cells, which was well corresponding to previous reports.[40, 41] Therefore, the developed ECL biosensor could be applied in the monitoring of miRNA biomarkers from cancer cells.

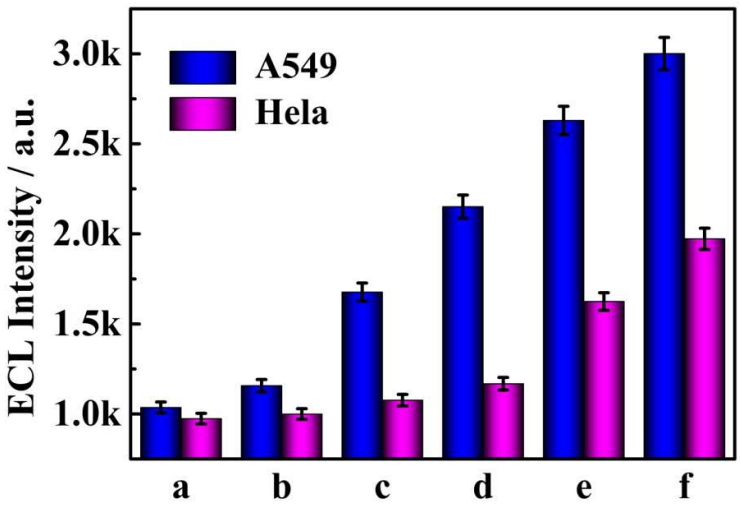

Figure 7 The application of the biosensor in different tumor cell lines detection: (a) 10 cells, (b) 10^2 cells, (c) 10^3 cells, (d) 10^4 cells, (e) 10^5 cells and (f) 10^6 cells of human lung adenocarcinoma cell line (A549) and human cervical cancer cell line (Hela), respectively. The ECL signals were measured in 0.1 M PBS (pH 7.4) containing 5 mM $K_2S_2O_8$ by scanning the potential from 0 to -1.35 V at a scanning rate of 100 mV/s.

CONCLUSIONS

In summary, DNA-stabilized Ag NCs were first *in situ* electrochemically generated on the product of the target-cycling synchronized RCA and applied in the ECL biosensor for ultrasensitive miR-21 detection. Significantly, the target-cycling synchronized RCA not only proposed a sensitive signal amplification strategy for the target cycle but also provided an efficient tandem periodic C-rich DNA as ligands for electrochemically generating Ag NCs. As expected, the DNA-stabilized Ag NCs presented nice and stable ECL property, which were employed to ultra-sensitively detect miR-21 with high specific response in practical tumor cells analysis. We believe the target-cycling synchronized RCA is of great significant to develop an efficient and convenient strategy for bioanalysis and the usage of the DNA-stabilized Ag NCs provides a new pattern to utilize Ag NCs in nanotechnology. Moreover, this proposed biosensor holds great potential for further application in biomedical research and early clinical diagnostics.

ASSOCIATED CONTENT

Supporting Information

The ideal structure of the padlock probe, Tm test, the cyclic voltammogram of Ag NCs electrochemical generation, LOD calculation and the calibration curves for practical detection are provided as Supporting Information. This material is available free of charge *via* the Internet at http://pubs.acs.org.

AUTHOR INFORMATION

*** Corresponding authors**

Tel.: +86 23 68252277, fax: +86 23 68253172.

E-mail addresses: yingzhuo@swu.edu.cn (Y. Zhuo), yuanruo@swu.edu.cn (R. Yuan).

Notes

The authors declare no competing financial interest.

ACKNOWLEDGMENT

This work was financially supported by the NNSF of China (21275119, 51473136，21575116), and the Fundamental Research Funds for the Central Universities (XDJK2015A002, XDJK2014A012), China.

REFERENCES

(1) Hu, L.; Xu, G. *Chem. Soc. Rev.* **2010**, 39, 3275-3304.

(2) Richter, M. M. *Chem. Rev.* **2004**, 104, 3003-3036.

(3) Miao, W. *Chem. Rev.* **2008**, 108, 2506-2553.

(4) Ding, Z. F.; Quinn, B. M.; Haram, S. K.; Pell, L. E.; Korgel, B. A.; Bard, A. J. *Science* **2002**, 296, 1293-1297.

(5) Zheng, L.; Chi, Y.; Dong, Y.; Lin, J.; Wang, B. *J. Am. Chem. Soc.* **2009**, 131, 4564-4565.

(6) Hesari, M.; Swanick, K. N.; Lu, J.-S.; Whyte, R.; Wang, S.; Ding, Z. *J. Am. Chem. Soc.* **2015**, 137, 11266-11269.

(7) Liu, Y.; Ai, K.; Cheng, X.; Huo, L.; Lu, L. *Adv. Funct. Mater.* **2010**, 20, 951-956.

(8) Richards, C. I.; Choi, S.; Hsiang, J.-C.; Antoku, Y.; Vosch, T.; Bongiorno, A.; Tzeng, Y.-L.; Dickson, R. M. *J. Am. Chem. Soc.* **2008**, 130, 5038-5039.

(9) Santiago Gonzalez, B.; Rodriguez, M. J.; Blanco, C.; Rivas, J.; Lopez-Quintela, M. A.; Gaspar Martinho, J. M. *Nano letters* **2010**, 10, 4217-4221.

(10) Shang, L.; Azadfar, N.; Stockmar, F.; Send, W.; Trouillet, V.; Bruns, M.; Gerthsen, D.; Nienhaus, G. U. *Small* **2011**, 7, 2614-2620.

(11) Wei, W.; Lu, Y.; Chen, W.; Chen, S. *J. Am. Chem. Soc.* **2011**, 133, 2060-2063.

(12) Hesari, M.; Ding, Z.; Workentin, M. S. *Organometallics* **2014**, 33, 4888-4892.

(13) Hesari, M.; Workentin, M. S.; Ding, Z. *Chem. Eur. J.* **2014**, 20, 15116-15121.

(14) Hesari, M.; Workentin, M. S.; Ding, Z. *Acs Nano* **2014**, 8, 8543-8553.

(15) Hesari, M.; Workentin, M. S.; Ding, Z. *Chem. Sci.* **2014**, 5, 3814-3822.

(16) Liu, T.; Zhang, L.; Song, H.; Wang, Z.; Lv, Y. *Luminescence* **2013**, 28, 530-535.

(17) Li, L.; Liu, H.; Shen, Y.; Zhang, J.; Zhu, J.-J. *Anal. Chem.* **2011**, 83, 661-665.

(18) Tao, Y.; Ran, X.; Ren, J.; Qu, X. *Small* **2014**, 10, 3667-3671.

(19) Liu, X.; Hu, R.; Gao, Z.; Shao, N. *Langmuir* **2015**, 31, 5859-5867.

(20) Petty, J. T.; Sergev, O. O.; Kantor, A. G.; Rankine, I. J.; Ganguly, M.; David, F. D.; Wheeler, S. K.; Wheeler, J. F. *Anal. Chem.* **2015**, 87, 5302-5309.

(21) Zhang, L. B.; Guo, S. J.; Zhu, J. B.; Zhou Z. X; Li, T.; Li, J.; Dong, S. J.; Wang, E. K. *Anal. Chem.* **2015**, 87, 11295−11300.

(22) Enkin, N.; Wang, F.; Sharon, E.; Albada, H. B.; Willner, I. *Acs Nano* **2014**, 8, 11666-11673.

(23) Orbach, R.; Guo, W.; Wang, F.; Lioubashevski, O.; Willner, I. *Langmuir* **2013**, 29, 13066-13071.

(24) Dean, F. B.; Nelson, J. R.; Giesler, T. L.; Lasken, R. S. *Genome Res.* **2001**, 11, 1095-1099.

(25) Han, D.; Wu, C.; You, M.; Zhang, T.; Wan, S.; Chen, T.; Qiu, L.; Zheng, Z.; Liang, H.; Tan, W. *Nat. Chem.* **2015**, 7, 835-841.

(26) Xu, F.; Shi, H.; He, X.; Wang, K.; He, D.; Guo, Q.; Qing, Z.; Yan, L.; Ye, X.; Li, D.; Tang, J. *Anal. Chem.* **2014**, 86, 6976-6982.

(27) Ge, J.; Zhang, L. L.; Liu, S. J.; Yu, R. Q.; Chu, X. *Anal. Chem.* **2014**, 86, 1808-1815.

(28) Harcourt, E. M.; Kool, E. T. *Nucleic Acids Res.* **2012**, 40, e65.

(29) Zhang, P.; Wu, X. Y.; Yuan, R.; Chai, Y. Q. *Anal. Chem.* **2015**, 87, 3202−3207.

(30) Liu, H.; Li, L.; Duan, L.; Wang, X.; Xie, Y.; Tong, L.; Wang, Q.; Tang, B. *Anal. Chem.* **2013**, 85, 7941-7947.

(31) Rashidnadimi, S.; Hung, T. H.; Wong, K.-T.; Bard, A. J. *J. Am. Chem. Soc.* **2008**, 130, 634-639.

(32) Nepomnyashchii, A. B.; Pistner, A. J.; Bard, A. J.; Rosenthal, J. *J. Phys. Chem. C* **2013**, 117, 5599-5609.

(33) Swanick, K. N.; Sandroni, M.; Ding, Z.; Zysman-Colman, E. *Chem. Eur. J.* **2015**, 21, 7435-7440.

(34) Dong, H.; Jin, S.; Ju, H.; Hao, K.; Xu, L.-P.; Lu, H.; Zhang, X. *Anal. Chem.* **2012**, 84, 8670-8674.

(35) Lu, Y.; Chen, W. *J. Power Sources* **2012**, 197, 107-110.

(36) Riskin, M.; Basnar, B.; Chegel, V. I.; Katz, E.; Willner, I.; Shi, F.; Zhang, X. *J. Am. Chem. Soc.* **2006**, 128, 1253-1260.

(37) Long, G. L.; Winefordner, J. D. *Anal. Chem.* **1983**, 55, 712A−724A.

(38) Wang, Z.; Si, L.; Bao, J.; Dai, Z. *Chem. Commun.* **2015**, 51, 6305-6307.

(39) Dong, H.; Hao, K.; Tian, Y.; Jin, S.; Lu, H.; Zhou, S.-F.; Zhang, X. *Biosens. Bioelectron.* **2014**, 53, 377-383.

(40) Liao, Y.; Huang, R.; Ma, Z.; Wu, Y.; Zhou, X.; Xing, D. *Anal. Chem.* **2014**, 86, 4596-4604.

(41) Yin, B. C.; Liu, Y. Q.; Ye, B. C. *J. Am. Chem. Soc.* **2012**, 134, 5064-5067.

For TOC Only

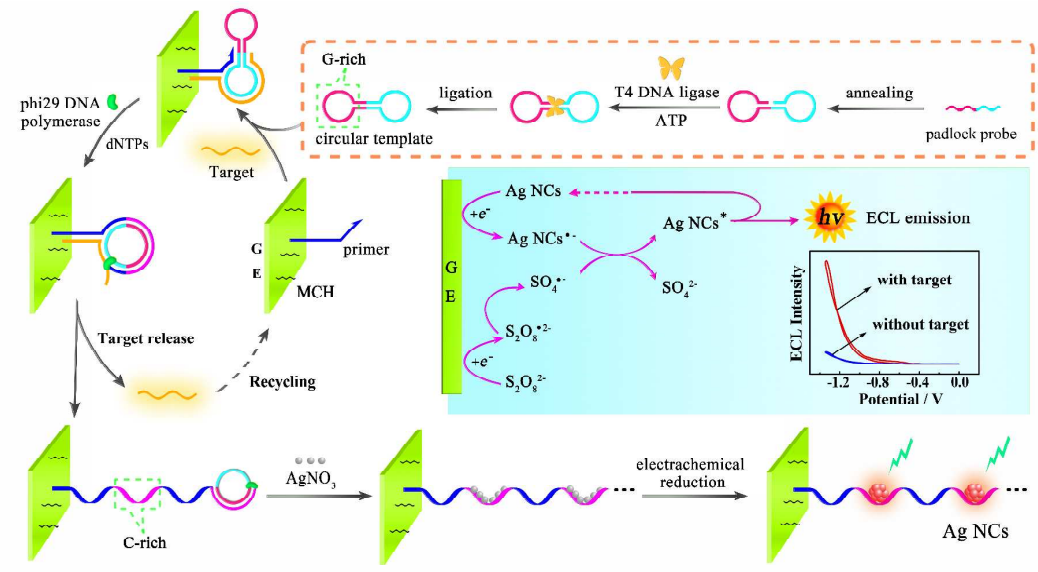
phi29 DNA polymerase
dNTPs
Target
G-rich
ligation
T4 DNA ligase
ATP
annealing
circular template
padlock probe
G E
primer
MCH
Target release
Recycling
Ag NCs
+e⁻
Ag NCs•⁻
Ag NCs*
hv
ECL emission
SO4•⁻
SO4²⁻
S2O8•²⁻
+e⁻
S2O8²⁻
ECL Intensity
with target
without target
-1.2 -0.8 -0.4 0.0
Potential / V
C-rich
AgNO3
electrachemical reduction
Ag NCs